Electric Power Systems Research 127 (2015) 177–185

Contents lists available at ScienceDirect

Electric Power Systems Research

journal homepage: www.elsevier.com/locate/epsr

Simulation of three-phase transformer inrush currents by using backward and numerical differentiation formulae

Amir Tokić [a], Viktor Milardić [b,*], Ivo Uglešić [b], Admir Jukan [a]

[a] Faculty of Electrical Engineering, Tuzla University, Tuzla 75000, Bosnia and Herzegovina
[b] Faculty of Electrical Engineering and Computing, University of Zagreb, Zagreb 10000, Croatia

ARTICLE INFO

Article history:
Received 28 November 2014
Received in revised form 31 March 2015
Accepted 24 May 2015

Keywords:
Three-phase transformer inrush currents
Numerical oscillations
L-stability
Extremely stiff system
Backward differentiation method

ABSTRACT

This paper presents a simplified model of a three-phase transformer developed in the state-space form using the linear graph theory. The algorithm for generating the coefficient matrixes of the state-space equation is described. Stiff detection procedures of differential equation systems that describe the three-phase transformer inrush current transients are explained. It is shown that the time-domain transient response of three-phase transformers mathematically describes extremely stiff systems. The numerical integration methods based on strong stable (*A* and *L*) backward differentiation formulae are used to solve extremely stiff differential equation systems arising from the state-space formulation of the transformer inrush current transient equations. A comparison of the measured and simulated three-phase transformer inrush currents showed very good agreement. The proposed procedure of modeling and the simulation method are useful tools that can be applied to other electrical transients where extremely stiff systems appear.

1. Introduction

The transformer is one of the most important elements of power systems. It is important to make a valid transformer model in the observed transient electromagnetic phenomena. There are different models of transformers depending on the frequency spectra of transients [1]. According to [2], the transformer inrush current belongs to the low-frequency transients, frequency up to 1 kHz. The transformer inrush currents are low-frequency electromagnetic transients that occur during energization of unloaded transformers. Depending on the transformer parameters, residual flux and the moment of switching on, the magnetic flux can reach a twice higher value in comparison with the rated operating value.

When the transformer is switched on and the value of the residual flux is near the point of saturation, the reduction of the transformer impedance to winding resistance and low inductance may occur in the saturation region of the magnetization curve. A direct consequence of this scenario is the iron core saturation and the production of transformer inrush currents. Inrush currents, which may be several times higher than the rated currents, can reduce the power quality due to voltage sag [3], cause the false operation of protective relays or fuses [4], damage the transformer windings due to developed mechanical forces [5] and in some scenarios cause harmonic resonance overvoltages [6,7].

Significant work has been done on developing the transformer models for the inrush current analysis. Several approaches to the modeling of the transformer in the time domain suitable for inrush current simulations are given in papers [8–15]. In general, a transformer model can be separated into two main parts: the transformer windings and the transformer iron core. The first part has a linear and the second one has a nonlinear character. The time-domain modeling of transformers is possible using the nodal approach (used in EMTP-based programs) or state-space approach (used in MATLAB).

In addition to the problem of transformer modeling, it is very important to pay special attention to the choice of simulation algorithm. The solution algorithm depends on the choice of the appropriate numerical method used in the simulation procedure of the mathematical model. For example, the EMTP-based programs use the compensation method to solve the system solution [16]. The system is first solved using Thevenin's equivalents, ignoring the nonlinear elements. A possible problem of a compensation method is that the Thevenin's equivalent cannot always be determined due to possible floating network formulations. In addition, special problems may arise during the simulation of the transformer transients.

The main purpose of this paper is to present a simplified technique of the three-phase transformer modeling with suitable

* Corresponding author. Tel.: +385 1 6129976; fax: +385 1 6129890.
E-mail addresses: amir.tokic@untz.ba (A. Tokić), viktor.milardic@fer.hr (V. Milardić), ivo.uglesic@fer.hr (I. Uglešić), admir.jukan@untz.ba (A. Jukan).

http://dx.doi.org/10.1016/j.epsr.2015.05.020
0378-7796/

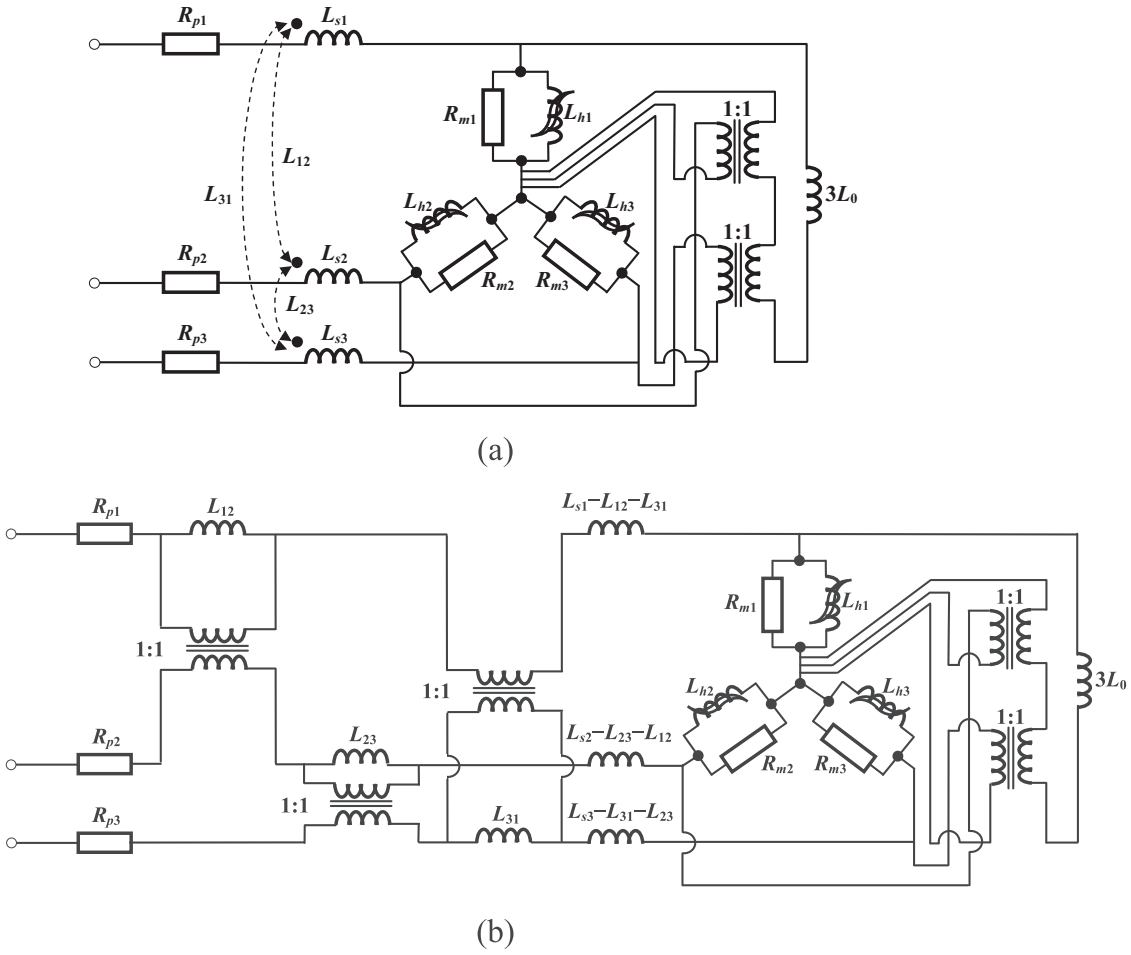

Fig. 1. *Three-phase transformer circuit model:* (a) the starting model which include mutual coupling between phases, (b) the equivalent circuit model.

solution algorithm based on the use of strongly stable numerical methods. The proposed numerical method was found to be strongly stable and accurate for the three-phase transformer inrush current simulations.

The reminder of this paper is organized as follows: in the following section the simplified circuit model of the three-phase, three-leg, two-winding transformer is explained. An algorithm for generating the state-space equations describing the three-phase transformer inrush current transients is developed in Section 3. The characteristics of the appropriated solution method based on backward differentiation formulae (BDF) or numerical differentiation formulae (NDF) are described in detail. The transformer inrush current measurements and numerical simulation results are compared in Section 4. The paper is concluded in Section 5.

2. Simplified transformer modeling procedure

The simplified circuit model of the three-phase, three-leg, and two-winding laboratory transformer with a star-star winding connection is shown in Fig. 1. The parameters of the circuit models can be obtained from standard open, positive and zero sequence tests. The proposed transformer model includes phase-to phase mutual coupling. This circuit model with additional zero sequence magnetizing inductance is the common simplified representation of a three-phase transformer in inrush current simulations [16,17].

Labels in Fig. 1 are: R_{pi} winding resistances, L_{si} winding leakage inductances, R_{mi} core loss resistors, L_{hi} core hysteretic inductors and L_0 zero sequence magnetizing inductance, $i = 1,2,3$.

The self inductance $L_s = L_{si}$ and mutual inductance $L_m = L_{ij}$ are calculated from positive (L_p) and zero (L_z) sequence values:

$$L_s = \frac{L_z + 2L_p}{3} \tag{1}$$

$$L_m = \frac{L_z - L_p}{3} \tag{2}$$

The starting model of the transformer is shown in Fig. 1(a), while the equivalent circuit model, which include mutual coupling between phases, is shown in Fig. 1(b).

In this part of the paper, particular attention will be devoted to the modeling of the nonlinear hysteretic inductor, Fig. 1(b). Normally, the nonlinear single-valued magnetization ($\phi - i_m$) or nonlinear multi-valued hysteresis ($\phi - i_h$) characteristics of iron core materials are typically modeled by piece-wise linear functions or some other nonlinear analytical functions. Common ways of modeling these nonlinear curves are to use a piece-wise linear function [18] or a polynomial [19], arctg [20] or hyperbolic function [21]. The use of nonlinear analytical functions in modeling nonlinear electrical components generally extends the simulation time of dynamic systems because of the Newton–Raphson iterative method, compared to the use of a piece-wise linear model. In addition, the use of curve-fitting extrapolation techniques can lead to problems in modeling the nonlinear inductance or hysteresis in a saturated area. On the other hand, the use of a piece-wise linear model is closely related to the appearance of unwanted overshooting effects [22].

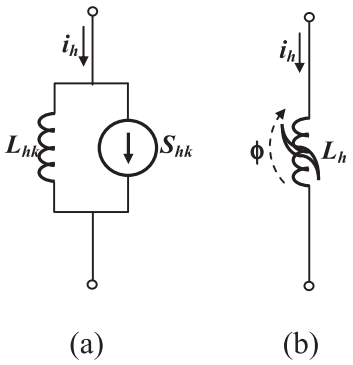

Fig. 2. (a) Nonlinear hysteretic inductor, (b) state-space model.

2.1. Modeling of hysteretic iron core inductor

In this paper, a modified approach to hysteretic inductor modeling is used, already shown in the paper [23]. Hysteretic inductor is defined by a set of points of one branch of the major hysteretic loop:

$$(i_{h_1}, \phi_{h_1}), \quad (i_{h_2}, \phi_{h_2}), \quad \ldots, \quad (i_{h_p}, \phi_{h_p})$$

where p is the total number of the sampled points of the (half) major hysteresis loop. It can be seen [24] that the final expression for magnetizing current of the kth piece-wise linear region of major loop in terms of the actual flux is:

$$i_h = \frac{1}{L_{h_k}}\phi + S_{h_k} \tag{3}$$

where there are, respectively:

$$L_{m_k} = \frac{\phi_{h_{k+1}} - \phi_{h_k}}{i_{h_{k+1}} - i_{h_k}}, \quad \Delta L_{m_k} = \frac{\operatorname{sgn}(\Delta\phi)\,\mu_k}{\operatorname{sgn}(\Delta\phi)\,\mu_k - 1} L_{m_k}, \quad L_{h_k} = L_{m_k} - \Delta L_{m_k}$$

$$\Delta I_k = \frac{1}{L_{m_k}}\eta_k, \quad S_{h_k} = \operatorname{sgn}(\Delta\phi) \times \left(I_{h_k} - \Delta I_k\right), \quad 1 \le k \le p-1$$

Finally, the nonlinear hysteretic inductor L_h in Fig. 2(a) is modeled through linear inductor L_{h_k} in parallel with an artificial current source S_{h_k}, Fig. 2(b).

The developed hysteretic inductor model takes into account the special operating conditions occurring due to the fact that the operating point in one particular case lies outside the major hysteresis loop. The developed model has a special subroutine for eliminating the possible overshooting effect [22,23].

3. Solution procedure for the three-phase transformer inrush current calculations

The developed models of nonlinear hysteretic inductors are very suitable for the development of state-space equation systems that describe low-frequency three-phase transformer transients such as transformer energization, Fig. 3. An arbitrary integration method could be applied in a state-space form. In the EMTP-ATP elements are strongly dependent on the integration step; this fact becomes apparent when a trapezoidal numerical rule is applied to the relevant branch.

It should be noted that some authors reported some numerical problems (numerical oscillations) during the simulation of the transformer transients [25–27]. In these works, the cause of the numerical problem is cited as 'stiff system' or 'nonlinearity of magnetizing curve'. However, these works do not explore in detail the causes of unwanted numerical oscillations, which is one of the main goals of this paper.

3.1. Modeling of the three-phase transformer transients

The algorithm procedure for generating state-space matrices is presented below. The standard state-space equation that describes transformer inrush current analysis is:

$$\frac{\mathrm{d}\boldsymbol{X}(t)}{\mathrm{d}t} = \boldsymbol{A}\,\boldsymbol{X}(t) + \boldsymbol{B}\,\boldsymbol{U}(t) = \boldsymbol{F}(\boldsymbol{X}, t) \tag{4}$$

The input vector contains the system voltages and current sources generated from nonlinear hysteretic inductors:

$$\boldsymbol{U}(t) = \begin{bmatrix} e_1 & e_2 & e_3 & S_{h_{1j}} & S_{h_{2k}} & S_{h_{3l}} \end{bmatrix}^T \tag{5}$$

In order to reach a solution of the standard state-space equation (2), and to generate the matrix of $\boldsymbol{A}$ and $\boldsymbol{B}$ coefficients, the theory of linear graphs will be used [24,28].

First, the proper graph tree is defined as a series of branches that connect all the nodes and it does not contain any loop. The remaining branches of the graph make a cotree, i.e. the connecting branches of the graph.

For electrical circuit model in Fig. 3, an appropriate graph with a properly defined tree or a cotree can be formed as in Fig. 4. Then, the variables of the system are defined as a current through the inductances that belong to the graph cotree. It should be noted that the graph in Fig. 4 contains the inductor cutset (marked in red) which reduces the dimension of the state vector i.e. the dimension of the whole system.

At the beginning, the state vector is defined as:

$$\tilde{\boldsymbol{X}}(t) = \begin{bmatrix} i_{L_1} & i_{L_2} & i_{L_0} & i_{h_{1j}} & i_{h_{2k}} & i_{h_{3l}} \end{bmatrix}^T \tag{6}$$

Customized equations of the state space can be written as:

$$\tilde{\boldsymbol{L}}\frac{\mathrm{d}\tilde{\boldsymbol{X}}(t)}{\mathrm{d}t} = \tilde{\boldsymbol{A}}\tilde{\boldsymbol{X}}(t) + \tilde{\boldsymbol{B}}\boldsymbol{U}(t) \tag{7}$$

where coefficients of matrices $\tilde{\boldsymbol{A}}$, $\tilde{\boldsymbol{B}}$ and $\tilde{\boldsymbol{L}}$ are unknown.

The elements of matrix $\tilde{\boldsymbol{A}}$ are obtained in stages, column by column. Hence, all voltage sources are short circuited, while all current sources and inductors are disconnected, excluding only the inductance through which the 1 A step source current flows. In the first three columns, currents are taken through ordinary inductors, while in the last three columns currents are taken through artificial linear hysteretic inductors.

The analogous procedure is used to determine the coefficients of matrix $\tilde{\boldsymbol{B}}$. In the first three columns, all current sources and inductors are disconnected, while all voltage sources are short circuited, excluding only the voltage source across which the 1 V step source is connected.

The last three columns are treated by analogy provided that all inductors and current sources are disconnected, excluding only the current source through which the 1 A step source current flows.

Elements of the matrices $\tilde{\boldsymbol{A}}$ and $\tilde{\boldsymbol{B}}$ are, respectively:

$$\tilde{\boldsymbol{A}} = \begin{bmatrix}
u_{L_1}\big|_{i_{L_1}=1} & u_{L_1}\big|_{i_{L_2}=1} & u_{L_1}\big|_{i_{L_0}=1} & u_{L_1}\big|_{i_{h_{1j}}=1} & u_{L_1}\big|_{i_{h_{2k}}=1} & u_{L_1}\big|_{i_{h_{3l}}=1} \\
u_{L_2}\big|_{i_{L_1}=1} & u_{L_2}\big|_{i_{L_2}=1} & u_{L_2}\big|_{i_{L_0}=1} & u_{L_2}\big|_{i_{h_{1j}}=1} & u_{L_2}\big|_{i_{h_{2k}}=1} & u_{L_2}\big|_{i_{h_{3l}}=1} \\
u_{L_0}\big|_{i_{L_1}=1} & u_{L_0}\big|_{i_{L_2}=1} & u_{L_0}\big|_{i_{L_0}=1} & u_{L_0}\big|_{i_{h_{1j}}=1} & u_{L_0}\big|_{i_{h_{2k}}=1} & u_{L_0}\big|_{i_{h_{3l}}=1} \\
u_{h_{1j}}\big|_{i_{L_1}=1} & u_{h_{1j}}\big|_{i_{L_2}=1} & u_{h_{1j}}\big|_{i_{L_0}=1} & u_{h_{1j}}\big|_{i_{h_{1j}}=1} & u_{h_{1j}}\big|_{i_{h_{2k}}=1} & u_{h_{1j}}\big|_{i_{h_{3l}}=1} \\
u_{h_{2k}}\big|_{i_{L_1}=1} & u_{h_{2k}}\big|_{i_{L_2}=1} & u_{h_{2k}}\big|_{i_{L_0}=1} & u_{h_{2k}}\big|_{i_{h_{1j}}=1} & u_{h_{2k}}\big|_{i_{h_{2k}}=1} & u_{h_{2k}}\big|_{i_{h_{3l}}=1} \\
u_{h_{3l}}\big|_{i_{L_1}=1} & u_{h_{3l}}\big|_{i_{L_2}=1} & u_{h_{3l}}\big|_{i_{L_0}=1} & u_{h_{3l}}\big|_{i_{h_{1j}}=1} & u_{h_{3l}}\big|_{i_{h_{2k}}=1} & u_{h_{3l}}\big|_{i_{h_{3l}}=1}
\end{bmatrix}$$

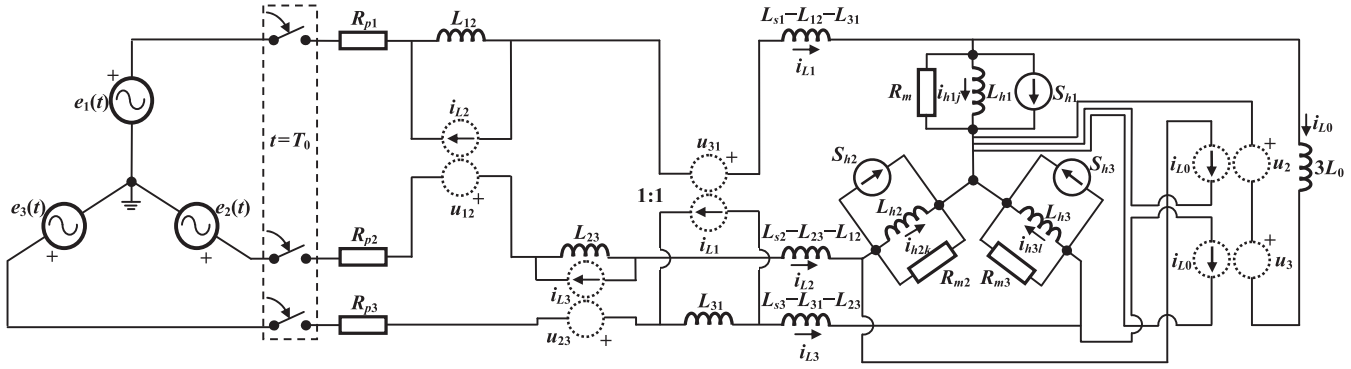

Fig. 3. Equivalent circuit model for transformer inrush current simulations.

$$\tilde{\boldsymbol{B}} = \begin{bmatrix} u_{L_1}|_{e_1=1} & u_{L_1}|_{e_2=1} & u_{L_1}|_{e_3=1} & u_{L_1}|_{S_{h_{1j}}=1} & u_{L_1}|_{S_{h_{2k}}=1} & u_{L_1}|_{S_{h_{3l}}=1} \\ u_{L_2}|_{e_1=1} & u_{L_2}|_{e_2=1} & u_{L_2}|_{e_3=1} & u_{L_2}|_{S_{h_{1j}}=1} & u_{L_2}|_{S_{h_{2k}}=1} & u_{L_2}|_{S_{h_{3l}}=1} \\ u_{L_0}|_{e_1=1} & u_{L_0}|_{e_2=1} & u_{L_0}|_{e_3=1} & u_{L_0}|_{S_{h_{1j}}=1} & u_{L_0}|_{S_{h_{2k}}=1} & u_{L_0}|_{S_{h_{3l}}=1} \\ u_{h_{1j}}|_{e_1=1} & u_{h_{1j}}|_{e_2=1} & u_{h_{1j}}|_{e_3=1} & u_{h_{1j}}|_{S_{h_{1j}}=1} & u_{h_{1j}}|_{S_{h_{2k}}=1} & u_{h_{1j}}|_{S_{h_{3l}}=1} \\ u_{h_{2k}}|_{e_1=1} & u_{h_{2k}}|_{e_2=1} & u_{h_{2k}}|_{e_3=1} & u_{h_{2k}}|_{S_{h_{1j}}=1} & u_{h_{2k}}|_{S_{h_{2k}}=1} & u_{h_{2k}}|_{S_{h_{3l}}=1} \\ u_{h_{3l}}|_{e_1=1} & u_{h_{3l}}|_{e_2=1} & u_{h_{3l}}|_{e_3=1} & u_{h_{3l}}|_{S_{h_{1j}}=1} & u_{h_{3l}}|_{S_{h_{2k}}=1} & u_{h_{3l}}|_{S_{h_{3l}}=1} \end{bmatrix}$$

Since the linear graph for the model contains inductor cutset, the elements of matrix $\tilde{\boldsymbol{L}}$ are obtained in a completely different way according to the redefined and generalized procedure described in the paper [22].

The procedure in the paper [22] could not solve the scenario of the appearance of the inductor cutset, the problem has been solved by inserting artificial elements in the original model of the system. The current sources are connected in series, in every branch of the cotree containing the inductances. Inductances in the tree remained in the original positions without adding the current sources. All other elements are removed from the electric circuit. Then matrix $\tilde{\boldsymbol{L}}$ is obtained in stages by type, so that the elements of the first type are obtained while maintaining the current source of the first inductance of the cotree until all current sources of the remaining inductances of the cotree are disconnected from the electric circuit.

The coefficients of the first type are obtained as equivalent inductance that is seen from cotree branches where there is the first inductance of the cotree. Analogously, the coefficients of other types are obtained as equivalent inductances that are seen from other cotree branches in which there are residual inductances of the cotree. The signs of the coefficient matrix $\tilde{\boldsymbol{L}}$ are obtained depending on the correlation of the voltage inductances in the branches of the cotree with the corresponding current through the inductances. The detailed procedure for obtaining the coefficients of the elements of the mentioned matrix is described in Ref. [24].

When the matrices $\tilde{\boldsymbol{A}}$, $\tilde{\boldsymbol{B}}$ and $\tilde{\boldsymbol{L}}$ are calculated according to previously described procedures, then the shift $\tilde{\boldsymbol{X}} = \boldsymbol{K}\boldsymbol{X}$, where $\boldsymbol{K}$ is a diagonal transformation matrix, i.e.

$$\boldsymbol{K} = \left[\mathrm{diag}(k_{i,i})\right]_{i=1,2,\ldots,6} \tag{8}$$

with elements:

$$k_{i,i} = 1, \quad i = 1, 2, 3, \quad k_{i,i} = \frac{1}{L_{h_{i(j,k,l)}}}, \quad i = 4, 5, 6$$

becomes the state vector containing the currents of the linear inductances and magnetic fluxes on the nonlinear hysteretic inductances:

$$\boldsymbol{X}(t) = \left[\, i_{L_1} \quad i_{L_2} \quad i_{L_0} \quad \phi_{1_j} \quad \phi_{2_k} \quad \phi_{3_l} \,\right]^T \tag{9}$$

Moving to the magnetic fluxes as state variables is suitable because, as integrals of the corresponding voltages, they are changed more smoothly than the corresponding currents.

Now Eq. (7) is written in the form:

$$\tilde{\boldsymbol{L}}\boldsymbol{K}\frac{\mathrm{d}\boldsymbol{X}(t)}{\mathrm{d}t} = \tilde{\boldsymbol{A}}\boldsymbol{K}\boldsymbol{X}(t) + \tilde{\boldsymbol{B}}\boldsymbol{U}(t) \tag{10}$$

The final equation obtained the form of a standard state-space equation (2), where the matrix of the system is obtained as

$$\boldsymbol{A} = (\tilde{\boldsymbol{L}}\boldsymbol{K})^{-1}\tilde{\boldsymbol{A}}\boldsymbol{K} \tag{11}$$

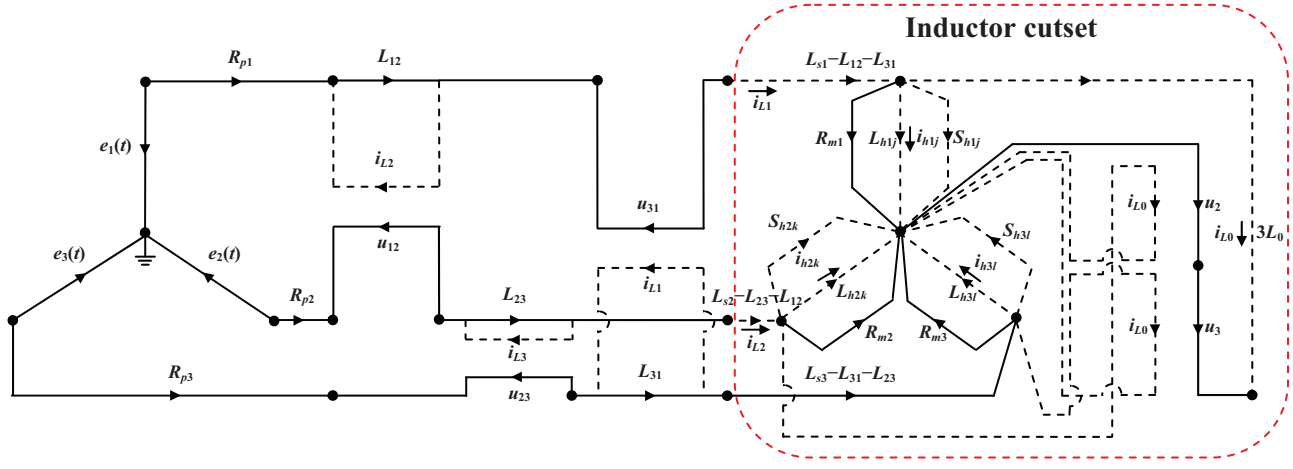

Fig. 4. Oriented graph for transformer circuit model. (For interpretation of the references to color in this figure legend, the reader is referred to the web version of this article.)

$$\boldsymbol{B} = (\tilde{\boldsymbol{L}}\boldsymbol{K})^{-1}\tilde{\boldsymbol{B}} \tag{12}$$

The matrices $\tilde{\boldsymbol{A}}$, $\tilde{\boldsymbol{B}}$, $\tilde{\boldsymbol{L}}$ and K are obtained according to the above described procedure:

$$\tilde{\boldsymbol{A}} = \begin{bmatrix} -2(R_p+R_m) & -(R_p+R_m) & 0 & R_m & 0 & -R_m \\ -(R_p+R_m) & -2(R_p+R_m) & 0 & 0 & R_m & -R_m \\ 0 & 0 & -3R_m & -R_m & -R_m & -R_m \\ R_m & 0 & -R_m & -R_m & 0 & 0 \\ 0 & R_m & -R_m & 0 & -R_m & 0 \\ -R_m & -R_m & -R_m & 0 & 0 & -R_m \end{bmatrix}$$

$$\tilde{\boldsymbol{B}} = \begin{bmatrix} 1 & 0 & -1 & R_m & 0 & -R_m \\ 0 & 1 & -1 & 0 & R_m & -R_m \\ 0 & 0 & 0 & -R_m & -R_m & -R_m \\ 0 & 0 & 0 & -R_m & 0 & 0 \\ 0 & 0 & 0 & 0 & -R_m & 0 \\ 0 & 0 & 0 & 0 & 0 & -R_m \end{bmatrix}$$

$$\tilde{\boldsymbol{L}} = \begin{bmatrix} 2(L_s-L_{13}) & L_s+L_{12}-L_{13}-L_{23} & 0 & 0 & 0 & 0 \\ L_s+L_{12}-L_{13}-L_{23} & 2(L_s-L_{23}) & 0 & 0 & 0 & 0 \\ 0 & 0 & 3L_0 & 0 & 0 & 0 \\ 0 & 0 & 0 & 1 & 0 & 0 \\ 0 & 0 & 0 & 0 & 1 & 0 \\ 0 & 0 & 0 & 0 & 0 & 1 \end{bmatrix},$$

$$\boldsymbol{K} = \begin{bmatrix} 1 & 0 & 0 & R_m & 0 & 0 \\ 0 & 1 & 0 & 0 & 0 & 0 \\ 0 & 0 & 1 & 0 & 0 & 0 \\ 0 & 0 & 0 & \dfrac{1}{L_{h_{1j}}} & 0 & 0 \\ 0 & 0 & 0 & 0 & \dfrac{1}{L_{h_{2k}}} & 0 \\ 0 & 0 & 0 & 0 & 0 & \dfrac{1}{L_{h_3 l}} \end{bmatrix}$$

The previously written matrix $\tilde{\boldsymbol{L}}$ is valid for a general (unsymmetrical) case of mutual coupling between phases.

In the case of $L_m = L_{ij}$, ($i,j = 1,2,3$, $i \neq j$) the following relation is obtained:

$$L_P = L_s - L_m \tag{13}$$

Now the matrix $\tilde{\boldsymbol{L}}$ can be written in the following form:

$$\tilde{\boldsymbol{L}} = \begin{bmatrix} 2L_p & L_p & 0 & 0 & 0 & 0 \\ L_p & 2L_p & 0 & 0 & 0 & 0 \\ 0 & 0 & 3L_0 & 0 & 0 & 0 \\ 0 & 0 & 0 & 1 & 0 & 0 \\ 0 & 0 & 0 & 0 & 1 & 0 \\ 0 & 0 & 0 & 0 & 0 & 1 \end{bmatrix}$$

Finally the matrices $\boldsymbol{A}$ and $\boldsymbol{B}$ are:

$$\boldsymbol{A} = \begin{bmatrix} -\dfrac{R_p+R_m}{L_p} & 0 & 0 & \dfrac{2R_m}{3L_pL_{h_{1j}}} & -\dfrac{R_m}{3L_pL_{h_{2k}}} & -\dfrac{R_m}{3L_pL_{h_{3l}}} \\ 0 & -\dfrac{R_p+R_m}{L_p} & 0 & -\dfrac{R_m}{3L_pL_{h_{1j}}} & \dfrac{2R_m}{3L_pL_{h_{2k}}} & -\dfrac{R_m}{3L_pL_{h_{3l}}} \\ 0 & 0 & -\dfrac{R_m}{L_0} & -\dfrac{R_m}{3L_0L_{h_{1j}}} & -\dfrac{R_m}{3L_0L_{h_{2k}}} & -\dfrac{R_m}{3L_0L_{h_{3l}}} \\ R_m & 0 & -R_m & -\dfrac{R_m}{L_{h_{1j}}} & 0 & 0 \\ 0 & R_m & -R_m & 0 & -\dfrac{R_m}{L_{h_{2k}}} & 0 \\ -R_m & -R_m & -R_m & 0 & 0 & -\dfrac{R_m}{L_{h_{3l}}} \end{bmatrix}$$

$$\boldsymbol{B} = \begin{bmatrix} \dfrac{2}{3L_p} & -\dfrac{1}{3L_p} & -\dfrac{1}{3L_p} & \dfrac{2R_m}{3L_p} & -\dfrac{R_m}{3L_p} & -\dfrac{R_m}{3L_p} \\ -\dfrac{1}{3L_p} & \dfrac{2}{3L_p} & -\dfrac{1}{3L_p} & -\dfrac{R_m}{3L_p} & \dfrac{2R_m}{3L_p} & -\dfrac{R_m}{3L_p} \\ 0 & 0 & 0 & -\dfrac{R_m}{3L_0} & -\dfrac{R_m}{3L_0} & -\dfrac{R_m}{3L_0} \\ 0 & 0 & 0 & -R_m & 0 & 0 \\ 0 & 0 & 0 & 0 & -R_m & 0 \\ 0 & 0 & 0 & 0 & 0 & -R_m \end{bmatrix}$$

It should be noted that, at every integration step, the matrix $\boldsymbol{A}$ is a function of the operating point position within all three major hysteresis loops, i.e.:

$$\boldsymbol{A} = \boldsymbol{A}(j,k,l) \tag{14}$$

3.2. Backward and numerical differentiation formulae

Before the application of any appropriate numerical method for the efficient simulation of the system, it is necessary to determine the character of the analyzed differential equation system (4). The equation system (4) can be nonstiff, stiff or an extremely stiff system. In general, a system is stiff if the eigenvalues (time constants) of the Jacobian system differ significantly in magnitude.

In this regard, the concept of stiffness is introduced, which is a specific characteristic of the system of differential equations related exclusively to solving the differential equation system using appropriate numerical methods. The practical measure of stiffness can be defined via the following quantitative parameters: stiffness ratio ξ and stiffness index ζ:

$$\xi = \frac{\max\limits_i \left| Re\left(\lambda_{j,k,l}^{(i)}\right)\right|}{\min\limits_i \left| Re\left(\lambda_{j,k,l}^{(i)}\right)\right|} \tag{15}$$

$$\zeta = \max_i \left| Re\left(\lambda_{j,k,l}^{(i)}\right)\right| \tag{16}$$

where $\lambda_{j,k,l}^{(i)}$, $i = 1, 2, \ldots, dim(\boldsymbol{A}(j,k,l))$ are eigenvalues of state matrices $\boldsymbol{A} = \boldsymbol{A}(j,k,l)$ calculated within every integration step. When $\xi \gg 1$, it is a stiff system and when $\zeta \to \infty$, it is an extremely or very stiff system. In other cases it is a nonstiff system. The numerical integration of stiff or very stiff systems by explicit numerical methods should be avoided, because these methods require an extremely small integration step to ensure numerical stability.

Stiff equation systems represent problems for which explicit methods do not work [29]. Regarding the second Dahliquist barrier, there are no explicit A-stable numerical methods, and implicit multistep methods can be A-stable if their order is at most 2 [29]. Implicit A- and L-stable numerical methods are required for the numerical integration of these kinds of systems [29,30].

The numerical methods of the second order of accuracy and their specific characteristics will be presented in the following text. The trapezoidal method is certainly the most widespread one in the simulations of the electrical systems. This method is very easy to implement because it is simple, *A*-stable of the second order and has the smallest error constant. The trapezoidal method applied to the state Eq. (2) is as follows:

$$\boldsymbol{X}_{n+1} = \boldsymbol{X}_n + \frac{\Delta t}{2}\left[\boldsymbol{F}(\boldsymbol{X}_n, t_n) + \boldsymbol{F}(\boldsymbol{X}_{n+1}, t_{n+1})\right] \tag{17}$$

However, a fundamental weakness of the trapezoidal method is associated with the occurrence of spurious numerical oscillations. Namely, the trapezoidal method is stable but not strong stable; more precisely, it has no characteristics of *L*-stability, so that during the simulation of extremely stiff systems, this method can give erroneous results. When using the trapezoidal method, the amplitude and frequency of the numerical oscillations depend on the parameters of energy storage elements and the integration step size, which is explored in detail in the paper [22]. The conclusion is that this method is advantageously used for the simulation of nonstiff or moderately stiff systems, while it should be avoided in the simulation of extremely stiff systems.

To overcome these problems, it is possible to use implicit backward Euler's method, since it is *L*-stable. However, this method is of the first order and it is insufficiently accurate in comparison with the trapezoidal method. The integration step size must be reduced to achieve the same accuracy as the trapezoidal method, which increases the simulation time.

On the other hand, the backward differentiation formulae of the *p*th order (BDF*p*) are the following [29–31]:

$$\sum_{m=1}^{p} \frac{1}{m} \nabla^m \boldsymbol{X}_{n+1} = \Delta t\, \boldsymbol{F}(\boldsymbol{X}_{n+1}, t_{n+1}) \tag{18}$$

BDF*p* are more accurate, and are $A(\alpha)$- and *L*-stable. *L*-stability properties of these methods damp out the response of the stiff and extremely stiff components, i.e. BDF suppresses the numerical oscillations.

The numerical differentiation formulae (NDF*p*) are fine-tuned BDF*p* with the following relations [32,33]:

$$\sum_{m=1}^{p} \frac{1}{m} \nabla^m \boldsymbol{X}_{n+1} = \Delta t\, \boldsymbol{F}(\boldsymbol{X}_{n+1}, t_{n+1}) + \kappa_p \gamma_p \left(\boldsymbol{X}_{n+1} - \boldsymbol{X}_{n+1}^{[0]}\right) \tag{19}$$

where parameter $\gamma_p = \sum_{m=1}^{p} \frac{1}{m}$, the starting value $X_{n+1}^{[0]} = \sum_{m=0}^{p} \nabla^m X_n$ and κ are the optimally chosen additional terms that retain maximum possible stability, reduce the truncation error and allow larger time step size. NDF*p* are also $A(\alpha)$- and *L*-stable.

The truncation error of BDF*p* can be approximated as

$$\varepsilon_{\mathrm{BDF}p} = \frac{1}{p+1} h^{p+1} \boldsymbol{X}^{(p+1)} \tag{20}$$

while the truncation error of NDF*p* can be approximated as

$$\varepsilon_{\mathrm{NDF}p} = \left(\kappa \sum_{m=1}^{p} \frac{1}{m} + \frac{1}{p+1}\right) h^{p+1} \boldsymbol{X}^{(p+1)} \tag{21}$$

It is clear that the integration step ensures a given accuracy. For the same defined tolerance of BDF*p* and NDF*p* method i.e. from $\varepsilon_{\mathrm{BDF}p} = \varepsilon_{\mathrm{NDF}p}$, a connection between the integration steps used in these two methods, $h_{\mathrm{BDF}p}$ and $h_{\mathrm{NDF}p}$, was obtained:

$$\frac{1}{p+1} h_{\mathrm{BDF}p}^{p+1} = \left(\kappa_p \gamma_p + \frac{1}{p+1}\right) h_{\mathrm{NDF}p}^{p+1} \tag{22}$$

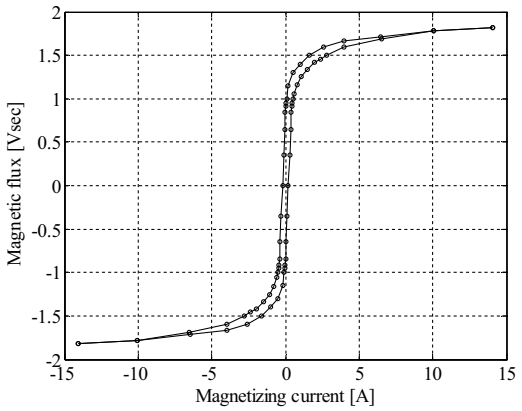

Fig. 5. Transformer hysteresis loop.

If the percentage of the change in integration steps of these two methods is marked with:

$$\delta_{p\%} = \frac{h_{\mathrm{NDF}p}^{p+1} - h_{\mathrm{BDF}p}^{p+1}}{h_{\mathrm{BDF}p}^{p+1}} \cdot 100\% \tag{23}$$

the following value is obtained:

$$\delta_{p\%} = \left[\left(\frac{1/(p+1)}{\kappa_p \gamma_p + \left(1/(p+1)\right)}\right)^{1/(p+1)} - 1\right] \cdot 100\% \tag{24}$$

NDF2 is *L*-stable method of the second order, so its relationship is $\delta_{2\%} = 26\,\%$. It can be concluded that the NDF2 is about 26% more efficient than the BDF2, and because of that NDF2 is the preferred method in this paper.

4. Three-phase transformer inrush currents: Measurements and simulations

The developed three-phase three-legged transformer equivalent circuit model is used for inrush current analysis (Fig. 4).

The electrical system parameters are ($i = 1,2,3$):

- source voltages: $e_i(t) = 311\cos(\omega t + i120^\circ - 155^\circ)$ V;
- rated system frequency: $f = 50$ Hz;
- transformer power rate: $S_{tr} = 2.4$ kV A;
- transformer ratio: $U_p/U_s = 0.38/0.5$ kV;
- short circuit voltage: $u_{k\%} = 3.0\%$;
- winding resistance: $R_{pi} = 1.5\ \Omega$;
- positive sequence inductance: $L_{pi} = 1.0$ mH;
- zero sequence inductance: $L_{zi} = 0.9$ mH;
- core loss resistance: $R_{mi} = 4626\ \Omega$;
- zero sequence magnetizing inductance: $L_0 = 5.0$ mH.

The major transformer hysteresis loop is shown in Fig. 5.

The presented measurements of three-phase transformer inrush currents were performed with MI 7111—Power Analyzer (sample rate: 256 S/period) and with FLUKE 434/5—Power Quality Analyzer (the maximum sampling rate 200 kS/s).

The accuracy levels of these devices are: MI 7111—Power Analyzer 0.1% plus 1 digit and FLUKE 434/5—Power Quality Analyzer 0.1%.

The moment of switching on ($T_0 = 3.10$ ms) was estimated, although there was dissipation between phases (3:05 ms, 3.12 ms, 3.15 ms). The source voltage was sine signal of fundamental frequency (50 Hz) although there were distortions of the phase voltages, i.e. THD of phase voltages were 2.62%, 2.80% and 2.83%, respectively.

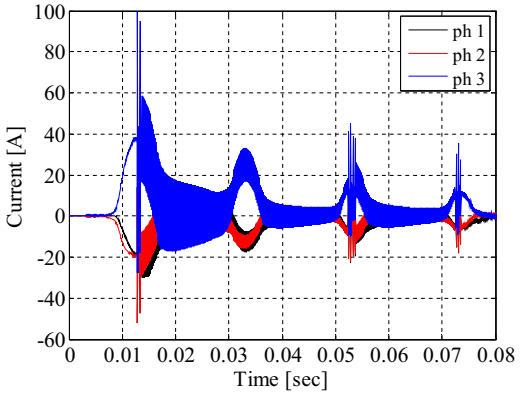

Fig. 6. Inrush current simulation, trapezoidal method, $\Delta t = 80\,\mu s$.

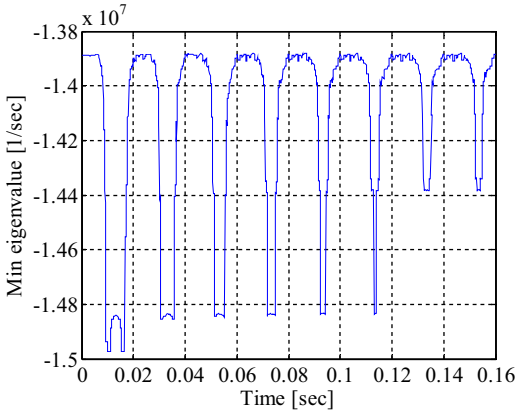

Fig. 7. Propagation of minimum real part of eigenvalues during the simulation time.

The simulation results of transformer inrush currents by using the classical trapezoidal method with integration step $\Delta t = 80\,\mu s$ are shown in Fig. 6.

The existence of the artificial numerical oscillations is evident by using the trapezoidal method. To detect the cause of these numerical oscillations in every integration step of the simulation, the maximal and minimal eigenvalues, as well as the stiffness ratio and stiffness index were computed. These results are shown in Figs. 7–9.

The limit values of defined stiffness parameters are obtained by the following:

$$1.388 \times 10^7 \le \zeta_{j,k} \le 1.497 \times 10^7$$

$$0.579 \times 10^6 \le \xi_{j,k} \le 6.947 \times 10^7$$

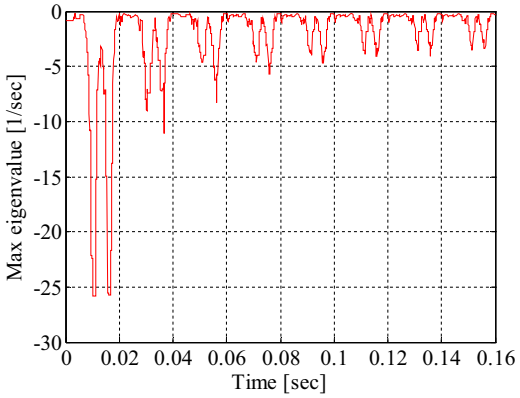

Fig. 8. Propagation of maximum real part of eigenvalues during the simulation time.

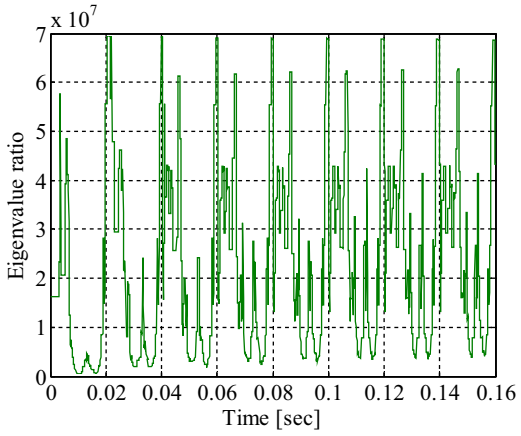

Fig. 9. Propagation of eigenvalue ratio during the simulation time.

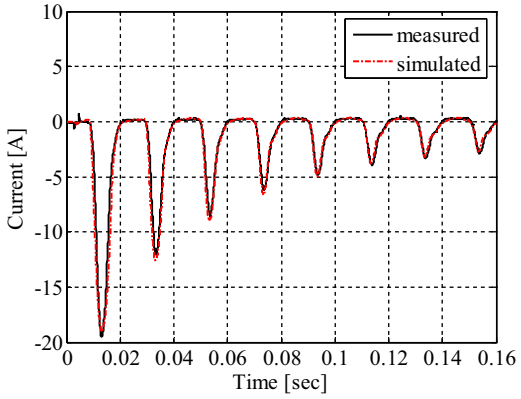

Fig. 10. Measured and simulated transformer inrush currents: phase 1.

It is clear that the state-space form of the transformer inrush current transients exhibits very stiff systems. Therefore, BDF2 and NDF2 methods were used for further simulations of the transformer energization.

The comparison between the measured and simulated transformer inrush currents is shown in Figs. 10–12. The simulations were performed by using the numerical method (NDF2) with the integration step size of $\Delta t = 80\,\mu s$.

The absolute difference between the measured and simulated transformer inrush currents as a function of time is shown in Figs. 13–15 according to the formula:

$$\varepsilon(t_k) = \left| i_{\text{simul.}}(t_k) - i_{\text{meas.}}(t_k) \right| \tag{25}$$

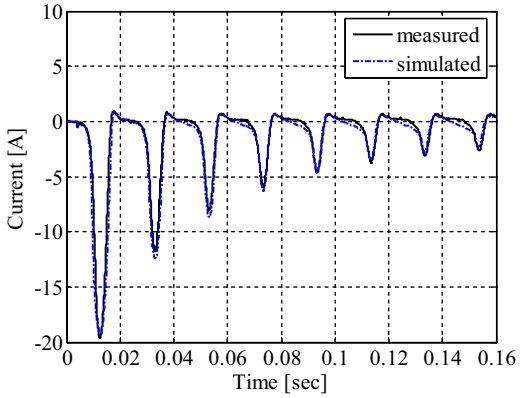

Fig. 11. Measured and simulated transformer inrush currents: phase 2.

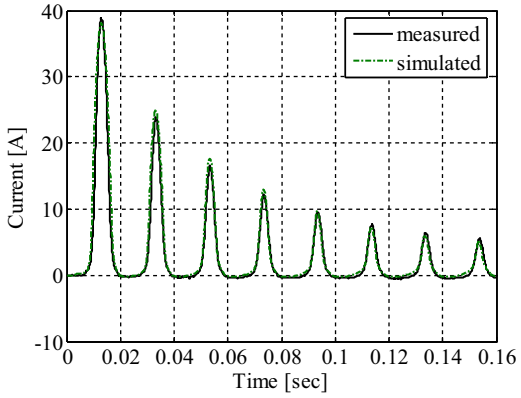

Fig. 12. Measured and simulated transformer inrush currents: phase 3.

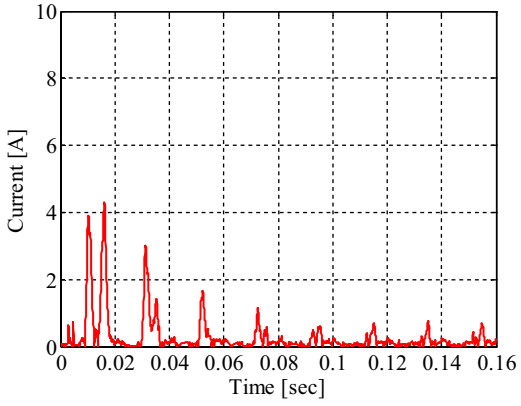

Fig. 13. Absolute difference between the measured and simulated transformer inrush currents: phase 1.

The propagation of the relative error of the transformer peak inrush currents is shown in Fig. 16. The relative error of current peak k, $1 \le k \le 8$ per phase $j = 1, 2, 3$ is calculated by relation:

$$\delta_j(k) = \frac{\left| i_{\text{simul.}}(k) - i_{\text{meas.}}(k) \right|}{i_{\text{meas.}j}} \cdot 100\% \tag{26}$$

where $i_{\text{meas}j} = \max_j \left\{ i_{\text{meas.}j}(k) \right\}$.

Based on the above explanation, it is possible to propose the implementation of the hybrid numerical method within the EMTP-based programs as a linear combination of the traditional trapezoidal method and the proposed BDF2 (NDF2) methods

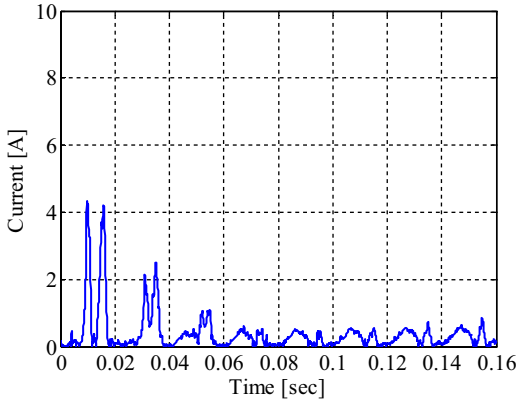

Fig. 14. Absolute difference the between measured and simulated transformer inrush currents: phase 2.

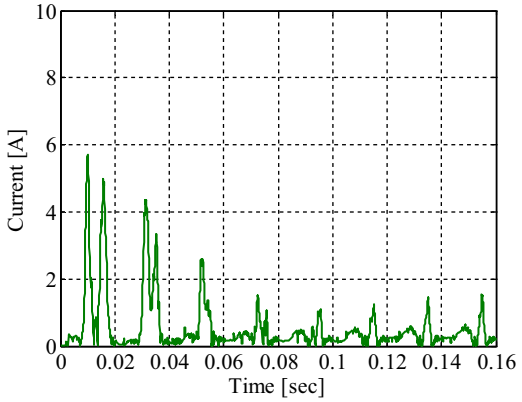

Fig. 15. Absolute difference between measured and simulated transformer inrush currents: phase 3.

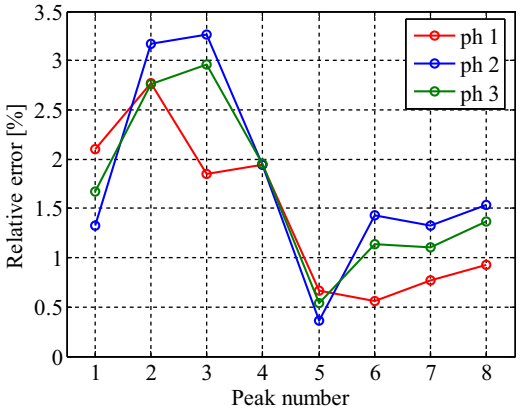

Fig. 16. Relative error of peak value of transformer inrush currents.

$0 \le \theta \le 1$:

$$\boldsymbol{X}_{n+1} = \left(1 + \frac{\theta}{3}\right)\boldsymbol{X}_n - \frac{\theta}{3}\boldsymbol{X}_{n-1} + \left(1 + \frac{\theta}{3}\right)\frac{\Delta t}{2}\boldsymbol{F}(\boldsymbol{X}_n, t_n) + (1-\theta)\frac{\Delta t}{2}\boldsymbol{F}(\boldsymbol{X}_{n+1}, t_{n+1}) \tag{27}$$

$$\boldsymbol{X}_{n+1} = \left(1 + \frac{\theta}{5}\right)\boldsymbol{X}_n - \frac{3\theta}{10}\boldsymbol{X}_{n-1} + (1-\theta)\frac{\Delta t}{2}\boldsymbol{F}(\boldsymbol{X}_n, t_n) + \left(1 + \frac{\theta}{5}\right)\frac{\Delta t}{2}\boldsymbol{F}(\boldsymbol{X}_{n+1}, t_{n+1}) + \frac{\theta}{10}\boldsymbol{X}_{n+1}^{[0]} \tag{28}$$

In expressions (27) and (28), $\theta = 0$ leads to the trapezoidal method, whereas $\theta = 1$ leads to the BDF2 (NDF2). In this way, it is possible to overcome some problems in using the standard trapezoidal method.

5. Conclusions

The simplified three-phase three-legged transformer model based on linear graph theory was developed in this paper. The model takes into account mutual coupling between the phases and hysteretic character of iron core.

The algorithm for generating system matrices in electrical networks is presented here. The analyzed network may contain inductor cut-sets and/or capacitor loops.

The main focus of the paper was to research the specific characteristics of the system of differential equations that describe the

three-phase transformer inrush current transients. In addition, the paper examined the corresponding numerical methods suitable for the simulation of extremely stiff systems. Based on the stiffness detection, it has been proven that the system of differential equations describing the three-phase transformer inrush current transient is an extremely stiff system that is solved by using methods based on backward differentiation formulae. The main cause of the stiffness of the system of differential equations is the dispersion of the parameters of the system as well as the nonlinearity of the hysteresis curve. The worst stiffness scenarios of the system are occurring at a time when the transformer iron core is in deep saturation.

Because of the stability properties of the mentioned BDF/NDF methods, it completely damps out unwanted numerical oscillations that are inherent in the classical trapezoidal method. The comparison of the measured and simulated three-phase transformer inrush currents showed very good agreement. Certainly, the authors are working on a more complex model of the transformer which will include the frequency dependence of the parameters. Further research will include asymmetric scenarios, i.e. a model of three-phase transformer that will take into account the equations of its magnetic circuits. The analog algorithm of generating system matrix and stiffness detection of the corresponding system of the differential equations will be applied in this model.

The proposed BDF/NDF methods have excellent qualities of accuracy and stability. The numerical methods are of the second order (local truncation error is of the same order as in the trapezoidal method) and are *A*- and *L*-stable. Additionally, NDF2 allows to use a 26% greater integration step than BDF2 to achieve the same accuracy.

In the paper the implementation of the hybrid method within the EMTP-type programs is suggested in order to overcome the numerical oscillations problems. This implementation refers to the general electrical networks which may alter the topology and parameters during the course of time so that the state equation may be non-stiff and stiff during the simulation and in this case it is interesting to use this hybrid rule. This will definitely be a special field of scientist's research in the future.

References

[1] CIGRE Working Group 33.02, Guidelines for Representation of Network Elements When Calculating Transients CIGRE Brochure 39, 1990.

[2] IEEE PES Task Force on Data for Modeling System Transients, Parameter determination for modeling system transients—Part III: Transformers, IEEE Trans. Power Delivery 20 (Jul (3)) (2005) 2051–2062.

[3] M.E. Golshan, M. Saghaian, A. Saha, H. Samet, A new method for recognizing internal faults from inrush current conditions in digital differential protection of power transformers, Electr. Power Syst. Res. 71 (2004) 61–71.

[4] M. Nagpal, T.G. Martinich, A. Moshref, K. Morison, P. Kundur, Assessing and limiting impact of transformer inrush current on power quality, IEEE Trans. Power Delivery 21 (April (2)) (2006) 890–896.

[5] M. Steurer, K. Fröhlich, The impact of inrush currents on the mechanical stress of high voltage power transformer coils, IEEE Trans. Power Delivery 17 (Jan (1)) (2002) 155–160.

[6] D. Povh, W. Schultz, Analysis of overvoltages caused by transformer magnetizing inrush current, IEEE Trans. Power Delivery PAS 97 (Jul/Aug (4)) (1978) 1355–1362.

[7] A. Tokić, I. Uglešić, Power quality problems due to transformer inrush current, in: Inter. CIGRE Symposium Transient Phenomena in Large Electric Power Systems, April 2007, Zagreb, Croatia, 2007, p. 8.

[8] J.A. Martinez, B.A. Mork, Transformer modeling for low- and mid-frequency transients—a review, IEEE Trans. Power Delivery 20 (Apr (2)) (2005) 1625–1632.

[9] B.A. Mork, F. Gonzalez, D. Ishchenko, D.L. Stuehm, J. Mitra, Hybrid transformer model for transient simulation—Part I: Development and parameters, IEEE Trans. Power Delivery 22 (1) (2007) 248–255.

[10] B.A. Mork, F. Gonzalez, D. Ishchenko, D.L. Stuehm, J. Mitra, Hybrid transformer model for transient simulation—Part II: Laboratory measurements and benchmarking, IEEE Trans. Power Delivery 22 (1) (2007) 256–262.

[11] E.P. Dick, W. Watson, Transformer models for transient studies based on field measurement, IEEE Trans. Power Appl. Syst. PAS-100 (1) (1981) 401–419.

[12] D. Dolinar, J. Pihler, B. Grcar, Dynamic model of a three-phase power transformer, IEEE Trans. Power Delivery 8 (Oct (4)) (1993) 1811–1819.

[13] C.E. Lin, J.C. Yeh, C.L. Huang, C.L. Cheng, Transient model and simulation in three-phase three-limb transformers, IEEE Trans. Power Delivery 10 (Apr (2)) (1995) 896–905.

[14] H. Mohseni, Multi-winding multi-phase transformer model with saturable core, IEEE Trans. Power Delivery 6 (1) (1991) 166–173.

[15] C.G.A. Koreman, Determination of the magnetizing characteristic of three-phase transformers in field tests, IEEE Trans. Power Delivery 4 (Jul (3)) (1989) 1779–1785.

[16] H.W. Dommel, Electromagnetic Transients Program Theory Book, Bonneville Power Admin, Portland, OR, USA, Aug. 1986.

[17] M. Kizilcay, Power System Transients and Their Computation, Univ. Appl. Sci. Osnabruck, Osnabruck, Germany, Jun. 2003.

[18] A. Tokić, I. Uglešić, G. Štumberger, Simulations of transformer inrush current by using BDF-based numerical methods, Math. Prob. Eng. 2013 (2013) 10.

[19] I.D. Mayergoyz, Mathematical Models of Hysteresis and Their Applications, Academic Press, Elsevier, New York, NY, USA, 2003.

[20] C. Pérez-Rojas, Fitting saturation and hysteresis via arctangent functions, IEEE Power Eng. Rev. (2000) 55–57.

[21] J. Takacs, A phenomenological mathematical model of hysteresis, COMPEL: Int. J. Comp. Math. Electr. Electron. Eng. 20 (4) (2001) 1002–1014.

[22] A. Tokić, I. Uglešić, Elimination of overshooting effects and suppression of numerical oscillations in transformer transient calculations, IEEE Trans. Power Delivery 23 (1) (2008) 243–251.

[23] A. Tokić, V. Madžarević, I. Uglešić, Hysteresis model in transient simulation algorithm based on BDF numerical method, in: Proc. of the IEEE Power Tech Conference, St. Petersburg, Russia, 2005, pp. 1–6.

[24] A. Tokić, Modeling, Simulation of Continuous Systems, PrintCom, Tuzla, BiH, 2011.

[25] S.G. Abdulsalam, W. Xu, V. Dinavahi, Modelling and simulation of three-phase transformers for inrush current studies, IEE Proc. Gener. Transm. Distrib. 152 (May (3)) (2005) 328–333.

[26] M. Vakilian, R.C. Degeneff, A method for modeling nonlinear core characteristics of transformers during transients, IEEE Trans. Power Delivery 9 (Oct (4)) (1994) 1916–1925.

[27] M. Vakilian, R.C. Degeneff, M. Kupferschmid, Computing the internal transient voltage response of a transformer with a nonlinear core using Gear's method, Part 1: Theory, IEEE Trans. Power Delivery 10 (Oct (4)) (1995) 1836–1842.

[28] D.B. West, Introduction to Graph Theory, Pearson Education, Inc, Singapore, 2002.

[29] E. Hairer, G. Wanner, Solving Ordinary Differential Equations II: Stiff and Differential-Algebraic Problems, Springer, Berlin, 2010.

[30] U. Ascher, L.R. Petzold, Computer Methods for Ordinary Differential Equations and Differential-Algebraic Equations, SIAM, Philadelphia, PA, 1998.

[31] C.W. Gear, Numerical Initial Value Problems in Ordinary Differential Equations, Prentice-Hall, Englewood Cliffs, NJ, USA, 1971.

[32] L.F. Shampine, M.W. Reichlet, The MATLAB ODE suite, SIAM—J. Numer. Anal. 18 (1) (1997) 1–28.

[33] R. Ashino, M. Nagase, R. Vaillancourt, Behind and beyond the MATLAB ODE suite, Comp. Math. Appl. 40 (2000) 491–512.